Desalination and Water Treatment
www.deswater.com
doi: 10.5004/dwt.2021.27624

235 (2021) 283–299
September

Efficient sequestration of Alizarin red from solution using a novel adsorbent based on zirconium and diethylenetriamine functionalized wheat straw

Jiajie Zhang[a], Jinghua Zhang[b,*], Mengmeng Yang[a], Runping Han[a,*]

[a]*College of Chemistry, Green Catalysis Center, Zhengzhou University, No 100 of Kexue Road, Zhengzhou, 450001 China, emails: rphan67@zzu.edu.cn (R. Han), 1270069595@qq.com (J. Zhang), 1582415059@qq.com (M. Yang)*
[b]*Department of Chemistry and Chemical Engineering, Huanghuai University, No. 599 of Wenhua Road, Zhumadian, 463000, China, email: hollyli@126.com*

Received 4 April 2021; Accepted 17 July 2021

ABSTRACT

In order to remove Alizarin red (AR) from solution, wheat straw was functionalized with diethylenetriamine and zirconium oxychloride octahydrate and modified wheat straw (Zr-DWS) was obtained. The materials were characterized using scanning electron microscopy, infrared spectroscopy, Brunauer–Emmet–Teller while the adsorption property of Zr-DWS toward AR was presented in batch mode and column mode. The results showed that Zr was successfully loaded on the surface of wheat straw. In order to clarify the reaction mechanism of the adsorption process, this work was carried out before and after adsorption. Zr-DWS can effectively adsorb AR from solution. The adsorption capacity of Zr-DWS for AR was 164 mg g^{-1} from experiment (pH = 6.2), and the increase of solution pH was not conducive to the adsorption process, but the effect of temperature was opposite. Pseudo-second-order kinetic model and Elovich equation can be used to describe the kinetic process, which shows that the adsorption is mainly chemical adsorption. The competitive adsorption between AR and acid chrome blue K (AK) shows that Zr-DWS has preferential adsorption performance for AR. Column adsorption results showed that high column, high concentration, and low flow rate were beneficial to the adsorption quantity of AR onto Zr-DWS. There was some regenerative property of spent Zr-DWS using 0.1 mol L^{-1} sodium hydroxide solution. Yan model can describe the column adsorption. Zr-DWS was effective and selective to remove AR from solution.

Keywords: Modified wheat straw; Alizarin red; Adsorption; Regeneration; Model analysis

1. Introduction

With the rapid development of industries such as textiles, leather and plastics, pollution caused by industrial activities has also become worrying [1,2]. Among them, wastewater is the main part of industrial waste, and dye wastewater produced by dyeing industry is considered to be the main polluting wastewater [3–5]. Dye molecules usually have complex aromatic structures and also have high chemical stability. They are inexpensive, have a wide variety of colors, and are widely used [6]. However, current studies have shown that dyes are highly toxic and non-biodegradable, and even at low level they possess carcinogenic, mutagenic and teratogenic effects [7,8]. In addition, most of the dyes make it difficult for sunlight to penetrate the water surface, thereby hindering the photosynthesis of aquatic plants, and even concentration less than 1 ppm in streams can cause aquatic life to die affecting the ecological balance [9,10]. In summary, the direct discharge of dye wastewater will cause serious water pollution and have a negative impact on human life and the environment. Therefore, it needs urgent attention to remove it from wastewater [11]. Traditional removal techniques include adsorption [12,13],

* Corresponding author.

flocculation [14] and precipitation [15], chemical oxidation, photocatalytic oxidation [16], electrochemical and biological methods. Among them, adsorption is widely regarded as one of the most economical and effective technologies for removal of dyes in wastewater.

The adsorption method is a simple and easy controllable method with significant advantages. In fact, it does not require any special equipment or pretreatment so can be applied to almost any type of dye wastewater treatment. The adsorption process is also very economical and environmental friendly, because they can be carried out under mild conditions, reducing the actual cost of the adsorbent, and different adsorbents can be selected according to the needs [17,18]. Membrane adsorbents, activated carbon, biological adsorbents and other types of adsorbents are used for the removal of organic dyes [19,20]. Among them, the adsorbents of modified biomass materials have great development potential for its advantages of biodegradability, eco-friendliness, and good adsorption performance.

Biomass adsorbents refer to agricultural by-products. They contain a large amount of cellulose and lignin, which are easily activated; they are cheap, easy to obtain, rich in variety, and environmental friendly, and are favored by more and more scholars. Biomass adsorbents mainly include straws (wheat straw [21], corn stalks [22], sorghum stalks, etc.), sycamore leaves, walnut shells, hazelnut shells, peanut shells [23], rice husks [24], bagasse and so on. These materials from biomass not only can be used to remove dyes and heavy metals in water but also can be converted into activated carbon for use. Zhang et al. [25] used the microwave method to treat peanut shells to make activated carbon to adsorb indigo carmine in water. The experiment proved that the adsorption effect is very good.

Wheat straw is a kind of simple and easy-to-obtain agricultural and forestry waste available in large quantities. Using wheat straw as an adsorbent has become a good way to reuse. Wu et al. [26] used natural wheat straw (NWS) to adsorb copper ion and methylene blue, and the adsorption capacity at 273 K and pH = 5 was 7.05 mg g^{-1}, respectively, indicating that there is some affinity about wheat straw toward positive ions. In most cases, NWS has a poor adsorption effect on dyes in water, so it is necessary to modify wheat straw to absorb pollutants in water.

The modification methods of wheat straw mainly include physical methods such as microwave method, ultrasonic method and carbonization method, and chemical methods such as alkali treatment, acid treatment, and surfactant method. The surface of wheat straw contains a lot of cellulose, hemicellulose, and a lot of hydroxyl active groups, so it is easy to be activated and modified. Wu et al. [27] used microwave-assisted wheat straw soaked in NaOH and pretreated with ethanol solution to remove Cd(II). Su et al. [28] used 1% cationic surfactant cetylpyridinium bromide (CPB) modified NWS to adsorb the bright green dye, the maximum theoretical adsorption capacity is 70.01 ± 3.39 mg g^{-1} at 293 K. Han et al. [29] used citric acid modified wheat straw to adsorb Cu^{2+} and MB in water, and the maximum theoretical adsorption capacity at 293 K was 39.17 and 396.9 mg g^{-1}, respectively [29].

Zirconium oxychloride octahydrate (ZOO) has been widely studied and used in wastewater treatment because of its abundant hydroxyl groups and good adsorption properties. ZOO forms an inner sphere complex through Lewis acid–base interaction, which shows a better removal effect. In addition, ZOO is nontoxic and easily available, also has low solubility in water [30], and it can be effectively regenerated in alkaline solutions, which means that it has great potential for water purification [31]. ZOO is usually in powder form and is difficult to separate and recover directly from water [32]. It is an effective method to overcome these shortcomings by loading ZOO on the support. Aryee et al. [33] used Fe_3O_4, iminodiacetic acid (IDA) and Zr to modify peanut husk to adsorb Alizarin red (AR). The adsorption capacity was 49.4 mg g^{-1} (at 313 K).

However, among these modification methods, there are few studies about Zr-loaded wheat straw for removal of pollutants. Therefore, the aim of this study was to prepare Zr-modified wheat straw to bind AR from solution. Characterization of wheat straw and modified straw was presented and adsorption property toward AR was performed in batch mode and column mode.

2. Materials and methods

2.1. Materials

The reagents used in the experiment are all analytically pure, including diethylenetriamine, epichlorohydrin, zirconium oxychloride ($ZrOCl_2·8H_2O$, Kermel, Tianjin, China), sodium hydroxide, hydrochloric acid, ethanol, sodium chloride, calcium chloride, sodium bicarbonate, Alizarin Red, Acid Chrome Blue K, the water used in the experiment is distilled water.

2.2. Preparation of adsorbent

- Preparation of DWS: First, the wheat straw was washed, dried, crushed, and 40–60 mesh was taken to obtain NWS. Then 1.5 g of NWS, 15 mL of CH_3CH_2OH, 30 mL of epichlorohydrin, and 200 mL of NaOH were taken in a 500-mL conical flask and shook using a 303-K thermostatic shaker for 3 h. Then it was taken out and 15 mL of CH_3CH_2OH and 15 mL of diethylene triamine were added in a 250-mL conical flask, shaken in a 303-K constant temperature shaker for 6 h and then left undisturbed for 24 h. It was then washed until neutral and dried to obtain DWS.
- Preparation of Zr-DWS: 1 g of $ZrOCl_2·8H_2O$ was dissolved in 50 mL water and the pH of the solution was adjusted until the solution has just precipitated. 1.000 g of DWS was added to the above solution and shaken at 303 K for 6 h. After the completion of the reaction, the solution was washed with distilled water until the solution had settled. Zr-DWS can be obtained by thermal drying.

2.3. Characterization of the adsorbent

In order to reasonably explain the experimental results and speculate the adsorption mechanism, the surface structure and physicochemical property of materials are measured.

The pH value of the zero charge point of materials was measured by the addition method of 0.010 mol L^{-1} sodium chloride solution. The characteristic functional groups were measured by Fourier transform infrared spectroscopy (PE-1710 FTIR infrared spectrometer, PE Company, USA). An element analyzer was used to determine the content of N, C, and H in the prepared wheat straw (Flash EA 1112 element analyzer, Thermo Electron Corporation, USA). The specific surface area of materials was evaluated by Brunauer–Emmet–Teller (BET) Analyzer (ASAP2420-4MP, USA). The surface morphology of wheat straw was confirmed by scanning electron microscopy (SEM) (Su8020 Hitachi Scanning Electron Microscope, Hitachi, Japan).

2.4. Adsorption experiment

2.4.1. Batch adsorption experiment

The batch adsorption experiments discussed the adsorption of AR solution under different conditions with Zr-DWS as the adsorbent. A series of optimizations were made to the experimental conditions, including the amount of adsorbent, salt concentration, pH value of the solution, reaction time, solution initial concentration, temperature, etc. And the corresponding models were used to fit the adsorption behavior and infer the mechanism. Eqs. (1) and (2) were used to calculate the adsorption quantity q (mg g^{-1}) of the adsorbent and the removal rate p (%) of the adsorbate.

$$q = \frac{V\left(C_0 - C\right)}{m} \tag{1}$$

$$p = \frac{\left(C_0 - C\right)}{C_0} \times 100\% \tag{2}$$

where m is the mass of Zr-DWS (g), V is the volume of the adsorbate solution (L), and C_0 and C are the adsorbate concentration in the solution before and after adsorption (mg L^{-1}).

The adsorption equilibrium study is to add 10 mg of Zr-DWS and AR solution with an initial concentration of 5–500 mg L^{-1} into a series of conical flask. Then shake in a shaker at temperatures of 293, 303, and 313 K, respectively. After 300 min, the mixture was centrifuged and the equilibrium concentration of AR in the solution was measured. The fitting analysis of the adsorption isotherm model can infer the mechanism of the adsorption process.

For equilibrium study, five adsorption isotherm models are used, namely Langmuir model, Freundlich model, Temkin model, Koble–Corrigan model and Redlich–Peterson model. Table 1 lists the expression of adsorption models.

2.6. Kinetic research

For kinetic study, add 10 mg Zr-DWS and 10 mL of AR solution with initial concentration of C_0 = 150, 250, 350 mg L^{-1} to a series of conical flasks. The mixture was shaken at 293, 303, and 313 K, respectively. The conical flask was taken out at different times, and the concentration of AR in the supernatant was determined after centrifugation. Adsorption kinetics studies the relationship between adsorption process and time. In this paper, the adsorption curve is fitted and analyzed by a pseudo-second-order kinetic model and Elovich equation. Table 1 lists the models used.

2.7. Thermodynamic parameters of Zr adsorption

The adsorption process is reversible. When the adsorption equilibrium is reached, the concentration of adsorbate in the solution will no longer change, and its apparent adsorption equilibrium constant (K_c) can be expressed as Eq. (3):

$$K_c = \frac{C_{\mathrm{ad},e}}{C_e} \tag{3}$$

where $C_{\mathrm{ad},e}$, C_e are the amount of adsorbate on the adsorbent and the amount of adsorbate remaining in the solution (mg L^{-1}) at equilibrium. Then use $\ln K_c$ to plot C_e, the intercept of the obtained line on the y-axis can be approximated as $\ln K_c^0$ under ideal conditions, and substituting the following formula to get changes in free energy (ΔG), entropy (ΔS) and enthalpy (ΔH).

$$\Delta G = -Rt \ln K_c^0 \tag{4}$$

$$\Delta G = \Delta H - T\Delta S \tag{5}$$

where R is the ideal gas constant (8.314 J mol^{-1} K^{-1}), and T is the absolute temperature in K.

2.4.2. Column adsorption experiment

The column adsorption experiment is to study the behavior of different concentrations of adsorbate solution flowing through the column at a certain flow rate, and the interaction between the adsorbate and the adsorbent in the column at different times. The research on the influence of Zr-DWS on the adsorption of AR is mainly from the column height, flow rate, initial concentration, and other factors in one fixed-bed mode. The operation is to take a certain quality of Zr-DWS and load it into a column with an inner diameter of 1 cm and a height of 40 cm. The AR solution was through column using a peristaltic pump. The experimental conditions are following: (1) bed height Z = 3.6 (0.435 g), 6.4 (0.725 g), and 8.6 cm (1.015 g), at pH = 3, C_{AR} = 600 mg L^{-1}, and flow rate v = 6.0 mL min^{-1}; (2) The flow rates were adjusted to v = 3.6, 6.0, and 8.4 mL min^{-1} with Z = 6.4 cm, pH = 3, C_{AR} = 600 mg L^{-1}; (3) Various AR concentration was performed (C_{AR} = 500, 600, 700 mg L^{-1}) at pH = 3, column height Z = 6.4 cm, flow rate v = 6.0 mL min^{-1}.

The concentration C_t of the adsorbate in the effluent at different time t (min) was measured until the value of C_t basically no longer changes. Plot C_t/C_0 and t to get the column adsorption penetration curve. The total adsorption amount Q_e (mg g^{-1}) and unit adsorption amount q_e (mg g^{-1}) of Zr-DWS are calculated by Eqs. (6) and (7).

$$Q_m = \frac{vC_0}{1{,}000}\left(t_{\mathrm{total}} - \int_{t=0}^{t=t_{\mathrm{total}}} \frac{C_t}{C_0} dt\right) \tag{6}$$

Table 1
Adsorption isotherms and kinetic models

Models	Nonlinear form	Parameters
Isotherm models		
Langmuir	$q_e = \frac{q_m K_L C_e}{1 + K_L C_e}$	K_L is equilibrium constant while qm is max adsorption quantity
Freundlich	$q_e = K_F C_e^{1/n}$	$1/n$ and K_F are constants of model
Koble–Corrigan model	$q_e = \frac{AC_e^n}{1 + BC_e^n}$	A, B and n are constants of model
Temkin model	$q_e = A + B\ln C_e$	A and B are constants of model
Redlich-Peterson model	$q_e = \frac{AC_e}{1 + BC_e^g}$	A, B and g ($0 < g < 1$) are constants of model
Kinetic models		
Pseudo-second-order	$q_t = \frac{k_2 q_e^2 t}{1 + k_2 q_e t}$	k_2 means rate constant (g mg^{-1} min^{-1}) while q_e is adsorption quantity of equilibrium (mg g^{-1})
Elovich	$q_t = A + B\ln t$	A and B are constants of model)
Column models		
Thomas model	$\frac{C_t}{C_0} = \frac{1}{1 + \exp\left(\left(k_{\mathrm{Th}} q_0 x / v\right) - k_{\mathrm{Th}} C_0 t\right)}$	k_{Th} is Thomas constant while q_0 is adsorption quantity (mg g^{-1})
Yan model	$\frac{C_t}{C_0} = 1 - \frac{1}{1 + \left(Q_t / b\right)^a}$	a and b are constants of model
Clark model	$\frac{C_t}{C_0} = \left(\frac{1}{1 + Ae^{-rt}}\right)^{1/(n-1)}$	A and r are constants while n is from Freundlich model

$$q_e = \frac{Q_m}{m} \tag{7}$$

The total mass W_{total} (mg) of the adsorbate flowing into the adsorption column and the removal rate Y (%) during the entire adsorption time t_{total} can be calculated by Eqs. (8) and (9).

$$W_{\mathrm{total}} = \frac{vC_0 t_{\mathrm{total}}}{1{,}000} \tag{8}$$

$$Y = \frac{Q_m}{W_{\mathrm{total}}} \times 100\% \tag{9}$$

2.7. Desorption and regeneration

2.7.1. Batch desorption regeneration

In order to make full use of the material, desorption and regeneration ability of the spent adsorbent was performed. First, the adsorbent is saturated, then the desorbed adsorbent is washed with distilled water until its surface is neutral, and different desorption solutions are selected to re-adsorb the desorbed adsorbent (the experimental operation is the same as the primary adsorption), and the unit adsorption capacity of the regenerated adsorbent is calculated as q_r. The desorption solution with the best effect was selected to carry out multiple desorption and regeneration of adsorbent. Desorption rate d and regeneration rate r are calculated according to Eqs. (10) and (11):

$$d = \frac{m_d}{m_0} \times 100\% \tag{10}$$

$$r = \frac{q_r}{q_m} \times 100\% \tag{11}$$

where m_d is the mass (mg) of adsorbate desorbed during desorption, and m_0 is the mass (mg) of adsorbent on adsorbent before desorption.

2.7.2. Column desorption and regeneration

The best desorption method in static desorption experiment was selected for desorption experiment of Zr-DWS

saturated with AR (the experimental conditions were the same as those in column adsorption experiment), and the concentration C_t (mg L^{-1}) of adsorbate in effluent at different time t (min) was measured until the concentration of effluent remained basically unchanged. Under the same experimental conditions, one more cycle regeneration was carried out. The desorption rate and regeneration rate of adsorbent are calculated, and the method is similar to batch desorption regeneration. The mass m_d (g) of adsorbate desorbed dynamically can be calculated by Eq. (12).

$$m_d = \frac{v}{1{,}000}\left(\int_{t=0}^{t=t_{\text{total}}} C_t dt\right) \tag{12}$$

In which v (mL L^{-1}) is the flow rate of desorption solution and t_{total} (min) is the total time of desorption reaction.

2.8. Competitive adsorption of AK and AR

In order to verify that the high adsorption capacity of Zr-DWS for AR is due to the selectivity of Zr (Zr complexed with the o-dihydroxy structure on AR benzene ring), this paper selected AK with different structure from AR (the two hydroxyl groups on the benzene ring are not adjacent) to do a comparative test of mixed components. Using 10 mL of AR, AK and their mixed solution with initial concentration of 300 mg L^{-1} and 10 mg Zr-DWS, the adsorption experiment was carried out. When measuring the concentration of the mixed solution of AK and AR, the λmax is 544 and 515 nm, respectively, and there is little difference between the two wavelengths, so the measurement method uses the dual-wavelength method to measure the absorbance, as follows:

$$c_A = \frac{k_{B_2}A_1 - k_{B_1}A_2}{k_{A_1}k_{B_2} - k_{A_2}k_{B_1}} \tag{13}$$

$$c_B = \frac{k_{A_2}A_2 - k_{A_2}A_1}{k_{A_2}k_{B_2} - k_{A_2}k_{B_1}} \tag{14}$$

where A_1 and A_2 are the total absorbance at 544 nm and 515 nm, respectively; k_{A1} and k_{A2} are the absorption coefficients of AR at 544m and 515 nm, respectively. k_{B1} and k_{B2} are the absorption coefficients of AK at 544 and 515 nm, respectively.

3. Results and discussion

3.1. Characterization of adsorbent

3.1.1. Determination of isoelectric point of adsorbent

NaCl solutions with the concentration of 0.01 mL L^{-1} were put into a series of flasks, and the pH value of the solutions was adjusted between 2.00 and 12.00 with 0.1 mL L^{-1} HCl and 0.1 mL L^{-1} NaOH. Then 0.010 g of the following adsorbents were added, and the solutions were shaken at 313 K for 12 h, and then separated with a sieve, and the pH value of the shaken solutions was determined. The change of ΔpH value of the solution before and after the reaction was calculated, and the plot of ΔpH vs. pH_0 was done. The intersection of the graph and horizontal axis is the isoelectric point (pH_{pzc}) of adsorbent. As shown in Fig. 1, the isoelectric points of NWS, DWS, and Zr-DWS are 7.4, 7.6, and 7.2, respectively.

It can be seen from Fig. 1 that the isoelectric point of natural wheat straw after modification moves to alkaline direction, because the alkaline groups of diethylenetriamine have been successfully loaded on the surface of wheat straw; After loading zirconium, the isoelectric point of wheat straw becomes smaller, which may be because zirconium is loaded on wheat straw in the form of complex, while zirconium oxide is an acidic group, which makes the isoelectric point of wheat straw move to acidic direction.

3.1.2. FTIR analysis

In order to compare the subtle differences of functional groups on the surface of adsorbents, several adsorbents were analyzed using FTIR, and the results are shown in Fig. 2.

It can be obviously seen from Fig. 2 that 1,730 cm^{-1} in NWS is the C=O stretching vibration of wheat straw,

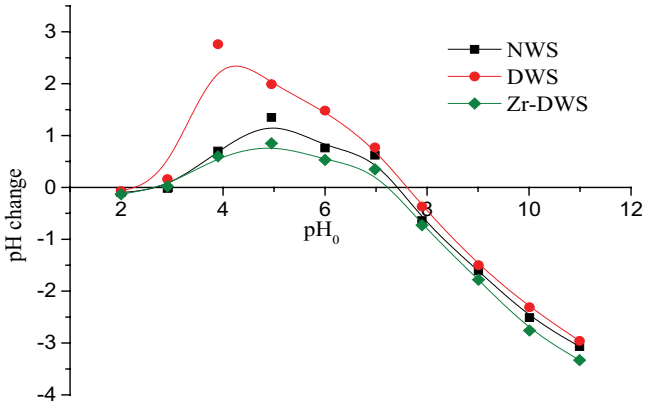

Fig. 1. Isoelectric point diagram of adsorbent before and after modification.

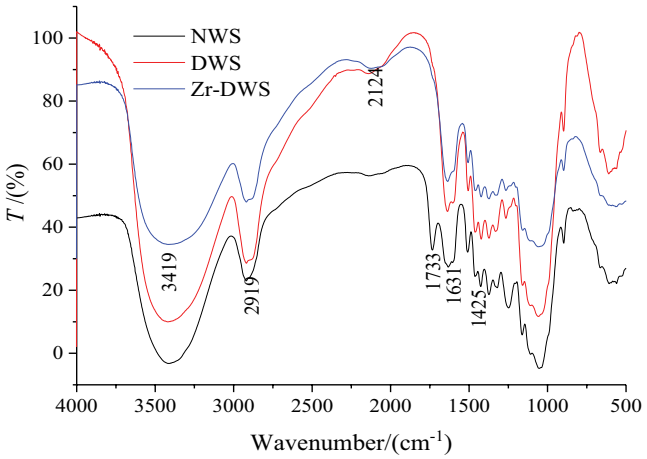

Fig. 2. Infrared spectra of adsorbent before and after modification.

1,509 cm^{-1} is the skeleton stretching vibration of benzene ring, 1,425 cm^{-1} is the stretching vibration of C–O, and 1,632 cm^{-1} is mainly the bending vibration of hydrated O–H bond. Compared with NWS, other materials disappeared at the peak of 1,730 cm^{-1}, mainly due to the action of sodium hydroxide, and the peak of 1,509 cm^{-1} moved to a low wavenumber, indicating that some lignin was destroyed [34]. Compared with NWS, the peak at 1,508 cm^{-1} in DWS is enhanced, which is due to the interaction between nitrogen-hydrogen bond and epoxy group to form –C–O–C [35], and there is an obvious absorption peak at 1,422 cm^{-1}, which is an amine absorption peak of –C–N, indicating that diethylenetriamine has been successfully loaded on wheat straw. The stretching vibration peak of –O–H bond of Zr-DWS is red shifted and widened, which may be related to the –OH of zirconium ion or the –OH of hydrated zirconium oxide on the surface of wheat straw; After loading zirconium, the peak at 1,632 cm^{-1} shifted to red, which may be caused by the binding of $[ZrO]^{2+}$, indicating that zirconium has been successfully loaded on wheat straw.

3.1.3. BET specific surface area analysis

The specific surface area of NWS and Zr-DWS is 2.09 and 0.759 $m^2\ g^{-1}$, respectively. So it can be seen that the specific surface area of wheat straw before and after modification is very small, and it decreases after modification, which may be due to the fact that amine and zirconium with larger groups block the internal microporous structure of wheat straw. This also corresponds to the fact that the adsorption of pollutants by wheat straw mainly depends on the action of surface groups instead of the surface area of wheat straw.

3.1.4. Scanning electron microscopy

In order to explore the changes of surface characteristics of wheat straw before and after modification, the adsorbent was analyzed by scanning electron microscope, as shown in Figs. 3a–c. First, adsorbent was sprayed with gold, and then its morphology was observed under electron microscope. It can be seen from the figure that the surface of the original wheat straw is rough and has many cavities, which is because the surface of the unmodified wheat straw contains cellulose, lignin, pectin, and hemicellulose, and the surface of Zr-DWS is smooth and the cellulose is arranged vertically and orderly.

3.2. Batch adsorption research

3.2.1. Determination of adsorbent dosage

The effect of adsorbent dosage on adsorption is evaluated in the range from 2 to 25 mg and the results are presented in Fig. 4. It was clearly seen from Fig. 4 that with the increase of adsorbent mass from 2 to 25 mg, the q_e of

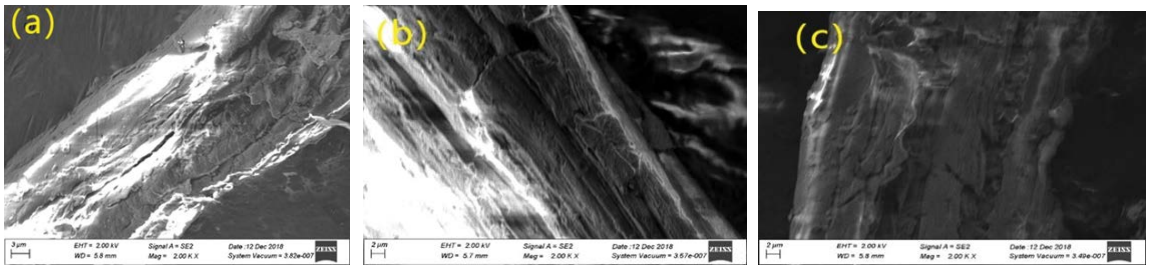

Fig. 3. Scanning electron microscopy micrographs of materials (a, b and c are NWS, DWS and Zr-DWS).

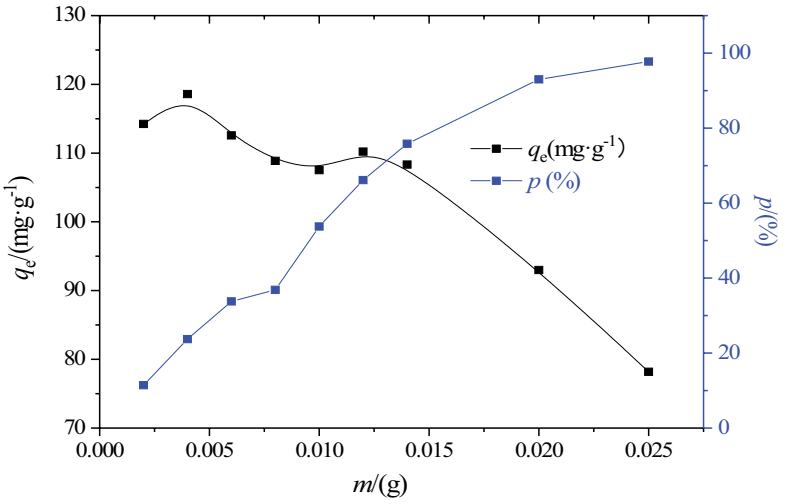

Fig. 4. Effect of Zr-DWS dosage on adsorption of AR (T = 303 K, t = 12 h, C_0 = 200 mg L^{-1}).

Zr-DWS for AR decreased from 115 to 78 mg g^{-1}, while the p increased from 11% to 97%. This is mainly because when AR in the solution is constant, with the increase of adsorbent, the active sites for adsorption of AR increase and the removal rate increases; However, with too more adsorbents, the number of AR solution molecules evenly distributed on each adsorbent decreases, and the adsorption capacity decreases. Therefore, considering comprehensively, the dosage of adsorbent in this experiment is 10 mg.

3.2.2. Effect of pH of solution

The pH of solution is a key factor for the adsorption property. So a series of experiments were performed to study the effect of pH on adsorption (Fig. 5).

It can be seen from Fig. 5 that with the increase of pH value, the adsorption capacity of Zr-DWS for AR first gradually decreases and then basically changes little. This is because when the solution pH < pH_{pzc} = 7.2, the surface of Zr-DWS is positively charged, and the increase of electrostatic attraction between AR as anionic dye and adsorbent is beneficial to its adsorption, so the lower the solution pH, the greater the adsorption capacity. When the pH of the solution changes from 2 to 10, the surface charge of Zr-DWS changes from positive to negative, and the attraction between Zr-DWS and AR weakens until it finally turns into repulsive force, so the adsorption capacity decreases, and the values of q_e are 173 mg g^{-1} at pH = 2 and 77.2 mg g^{-1} at pH = 10. But the solution still maintains a large adsorption capacity at pH 8~10 (q_e > 75 mg g^{-1}), which shows that the force between Zr-DWS and AR has other stronger forces besides electrostatic attraction, such as hydrogen bonding and complexation. Taking into account the pH of the actual dye wastewater, this paper does not adjust the pH but uses the original solution (pH = 6.2) for experimental research.

There is almost adsorption quantity of NWS toward AR. So there is improvement of adsorption capacity after modification.

3.2.3. Effect of salt concentration in solution

It is known that industrial wastewater contains some salt, so in order to evaluate the application of an adsorbent in actual wastewater remediation, it is necessary to evaluate its ionic strength. Fig. 6 describes the effect of salt concentration on adsorption quantity.

It can be seen from Fig. 6 that the surface of the adsorbent is positively charged at AR solution pH = 3. At this time, the attraction between Zr-DWS and AR mainly depends on the electrostatic attraction. The increase of salt makes Na^+ competitively adsorb with the adsorbent and reduces the adsorption capacity. Therefore, the salt solution has a negative effect on the adsorption. However, the change of the salt has basically no effect on Zr-DWS at pH = 6.2. This is because the solution is weakly acidic. At this time, Zr-DWS and AR mainly rely on complexation. Therefore, the presence of salt has some effect on the adsorption of AR by Zr-DWS. But at pH 9, the presence of salt has a slightly positive effect, and the concentration of salt has no effect on the adsorption of AR by Zr-DWS. This is because AR solution (dissociation constant pK_{a1} = 4.5, pK_{a2} = 11) has a part of negative charge under this condition. The presence of salt ions reduces the thickness of the electric double layer and makes it easier for AR to approach the active site, thereby increasing the adsorption capacity of AR. The Zr-DWS and AR under this condition are mainly connected by complexation. Therefore, the amount of salt in the solution has almost no effect on the adsorption of AR by Zr-DWS at higher solution pH.

3.2.4. Effect of AR concentration and adsorption isotherm studies

The study of the isothermal model can reflect the interaction between the adsorbates and the adsorbents, and provide a theoretical basis for inferring the reaction mechanism and adsorption capacity. The effect of AR concentration on adsorption quantity is presented in Fig. 7. It was clearly seen from Fig. 7 that the values of q_e became rapidly larger at the initial stage of curves, then changed small. Furthermore, it was also found that values of q_e became large with the increase of temperature. This confirmed that the process is endothermic. The max values of q_e from Fig. 7 are 152, 162 and 164 mg g^{-1} at 293, 303 and 313 K, respectively.

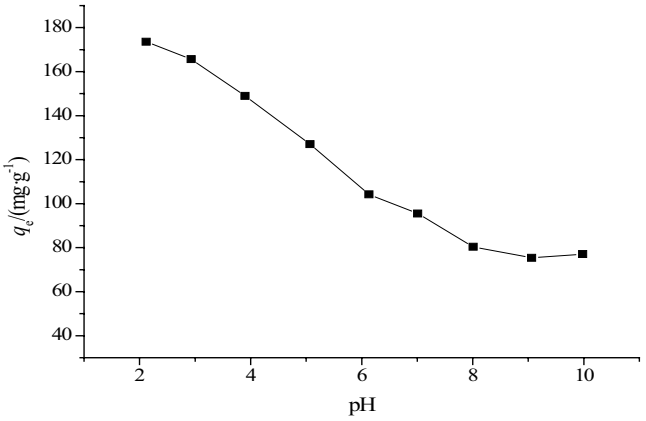

Fig. 5. Effect of pH value of solution on adsorption of AR (T = 303 K, m = 0.010 g, C_0 = 200 mg L^{-1}).

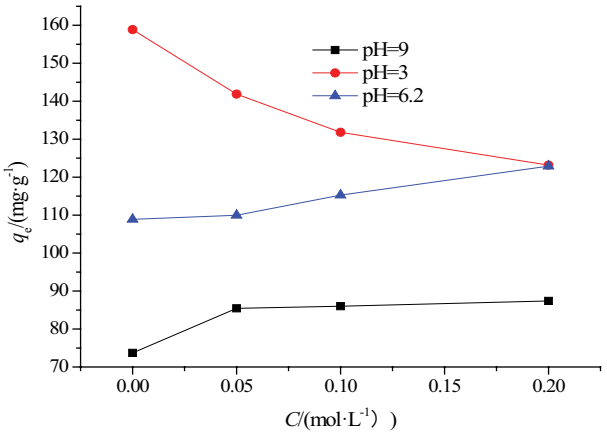

Fig. 6. Effect of salt concentration in solution on AR adsorption (T = 303 K, t = 12 h, C_0 = 200 mg L^{-1}).

Langmuir, Freundlich, Koble–Corrigan, Temkin and Redlich–Peterson models were used to analyze the adsorption isotherm of Zr-DWS adsorption of AR by nonlinear fitting. The fitting curves are also shown in Fig. 7, and the parameters obtained by fitting are shown in Table 2.

It was seen from Table 2 that the parameter K_L of Langmuir model increased with the increase of temperature, which indicated that the binding force between adsorbate and adsorbent was rising. This was consistent with the increasing trend of adsorption capacity with the increase of

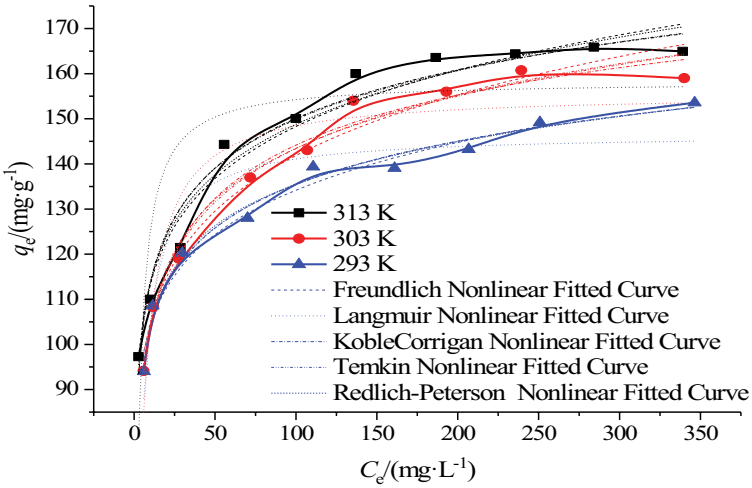

Fig. 7. Adsorption isotherms AR adsorption and fitted curves.

Table 2
Nonlinear fitting of isotherms of AR adsorption by Zr-DWS

Langmuir					
T/(K)	K_L/(L mg^{-1})	$q_{e(exp)}$/(mg g^{-1})	$q_{m(theo)}$/(mg g^{-1})	R^2	SSE × 10^2
293	0.251 ± 0.045	152	147 ± 3	0.867	0.426
303	0.204 ± 0.039	161	156 ± 4	0.879	0.502
313	0.378 ± 0.120	164	158 ± 5	0.727	1.408
Freundlich					
T/(K)	K_F	$1/n$		R^2	SSE × 10^2
293	81.0 ± 2.2	0.109 ± 0.006		0.981	0.612
303	77.6 ± 3.2	0.131 ± 0.009		0.971	1.19
313	86.6 ± 4.5	0.117 ± 0.011		0.942	2.97
Koble–Corrigan					
T/(K)	A	B	n	R^2	SSE × 10^2
293	105 ± 9	0.409 ± 0.190	0.218 ± 0.087	0.982	0.508
303	91.7 ± 7.9	0.409 ± 0.071	0.321 ± 0.098	0.980	0.692
313	114 ± 14	0.430 ± 0.250	0.243 ± 0.130	0.944	2.54
Temkin					
T/(K)	A	B		R^2	SSE × 10^2
293	71.8 ± 2.6	13.8 ± 0.6		0.985	0.482
303	64.6 ± 3.7	17.1 ± 0.8		0.981	0.768
313	77.9 ± 1.2	15.6 ± 1.2		0.948	2.69
Redlich–Peterson					
T/(K)	A	$B \times 10^3$	g	R^2	SSE × 10^2
293	1.85 ± 1.11	0.167 ± 0.089	0.909 ± 0.011	0.985	0.406
303	1.34 ± 0.94	0.120 ± 0.073	0.896 ± 0.019	0.977	0.826
313	8.15 ± 21.00	0.732 ± 0.200	0.890 ± 0.021	0.936	2.91

temperature. But the correlation coefficient was small (all below 0.9) and the relative error was larger. So it cannot be used to describe the adsorption process of AR by Zr-DWS. Other models were suitable for describing the adsorption process, which shows that the adsorption process is a heterogeneous multi-molecular layer adsorption. Parameter K_F from Freundlich model was no change rule while $1/n$ was between 0.1 and 0.5, indicating that adsorption was easy. Koble–Corrigan model was a combination of Langmuir model and Freundlich model. If the parameter $1/n$ was biased towards 0, the adsorption will be biased towards the Freundlich model, and if the parameter $1/n$ was biased towards 1, the adsorption will be biased towards Langmuir model. Parameter $1/n$ listed in table was biased towards 0, which was more in line with the Freundlich model. Temkin model can also describe the adsorption process.

Comprehensive analysis of R^2 and SSE shows that the adsorption of AR by Zr-DWS can be described by Freundlich, Koble–Corrigan, Temkin and Redlich–Peterson models except Langmuir model, but Koble–Corrigan model was more suitable for describing the adsorption process.

3.2.5. Adsorption kinetics

Effect of contact time on adsorption quantity is presented in Fig. 8 at various temperatures and AR concentration. It was noticed that the values of q_t became significantly larger at first stage, then slightly increased and finally reached equilibrium. It was also observed that there was higher adsorption quantity at higher temperature.

In order to speculate the mechanism of adsorption experiment, pseudo-first-order kinetic model, pseudo-second-order kinetic model and Elovich equation are used to fit the kinetic data of AR adsorption under different adsorption conditions, as shown in Fig. 8, and the fitted data are listed in Table 3.

It was shown that the pseudo-first-order kinetic model with larger values of SS was not used to describe the adsorption process. R^2 in pseudo-second-order kinetic model is greater than 0.96, and SSE is relatively small, which is the most suitable for describing the adsorption process, indicating that the adsorption process of Zr-DWS for AR is controlled by chemical adsorption. Elovich equation describes heterogeneous chemical adsorption, especially ion exchange process. The fitting results of kinetic data show that the adsorption process of AR by Zr-DWS contains heterogeneous ion exchange. To sum up, pseudo-second-order equation can best describe the adsorption process of AR by Zr-DWS, which is heterogeneous chemical adsorption and contains ion exchange process.

3.2.6. Thermodynamic analysis of adsorption

According to the formulae (7–9), the thermodynamic parameters of the adsorption process of AR on Zr-DWS can be calculated, and the results are shown in Table 4.

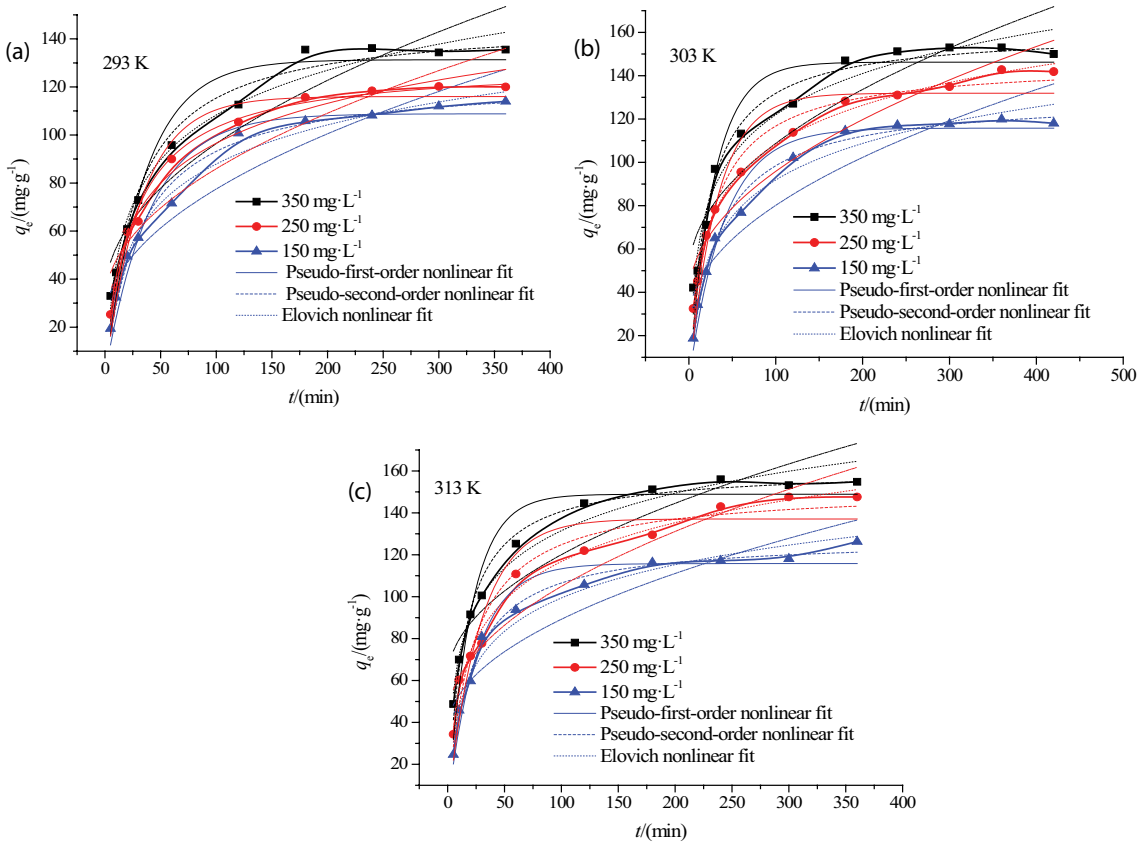

Fig. 8. Effect of contact time on AR adsorption and fitted curves.

Table 3
Kinetic nonlinear fitting parameters of AR adsorption by Zr-DWS

Pseudo-first-order kinetic model						
T/(K)	C_0/(mg L^{-1})	$q_{e(exp)}$ /(mg g^{-1})	$q_{e(theo)}$ /(mg g^{-1})	$k_1 \times 10^{-2}$ /(min^{-1})	R^2	SSE × 10^2
293	150	114	109 ± 3	2.47 ± 0.29	0.963	0.376
	250	120	116 ± 3	3.00 ± 0.31	0.967	3.45
	350	135	131 ± 5	2.81 ± 0.39	0.941	7.88
303	150	118	116 ± 3	2.46 ± 0.26	0.969	3.49
	250	141	132 ± 4	3.05 ± 0.44	0.929	10.2
	350	150	146 ± 4	3.45 ± 0.45	0.936	10.5
313	150	126	116 ± 3	3.84 ± 0.43	0.958	4.13
	250	147	137 ± 6	3.51 ± 0.58	0.905	12.5
	350	156	149 ± 5	4.81 ± 0.65	0.920	9.92
Pseudo–second–order kinetic model						
T/(K)	C_0/(mg L^{-1})	$q_{e(exp)}$/(mg g^{-1})	$q_{e(theo)}$/(mg g^{-1})	$k_2 \times 10^{-4}$	R^2	SSE × 10^2
293	150	114	124 ± 3	2.46 ± 0.28	0.988	1.18
	250	120	130 ± 3	2.97 ± 0.23	0.993	0.705
	350	135	147 ± 4	2.44 ± 0.35	0.978	2.93
303	150	118	130 ± 2	2.39 ± 0.22	0.991	1.12
	250	141	146 ± 3	2.70 ± 0.31	0.983	2.46
	350	150	161 ± 4	2.87 ± 0.35	0.970	0.589
313	150	126	128 ± 2	3.87 ± 0.35	0.990	0.971
	250	147	152 ± 5	3.05 ± 0.50	0.966	4.46
	350	156	161 ± 3	4.29 ± 0.41	0.975	0.461
Elovich equation						
T/(K)	C_0/(mg L^{-1})	$q_{e(exp)}$ /(mg g^{-1})	α/(g mg^{-1} min^{-1}) × 10^2	β/(g mg^{-1}) × 10^2	R^2	SSE × 10^2
293	150	114	42.1	4.30	0.986	1.40
	250	120	56.1	4.20	0.983	1.77
	350	135	56.3	3.70	0.979	2.83
303	150	118	43.8	4.10	0.982	2.32
	250	141	66.0	3.90	0.996	0.586
	350	150	84.8	3.60	0.971	4.74
313	150	126	76.0	4.40	0.976	2.35
	250	147	78.3	3.70	0.987	1.73
	350	156	162	3.90	0.974	3.18

Table 4
Thermodynamic parameters of Zr-DWS adsorption of AR

E_a/ (kJ mol^{-1})	ΔH/ (kJ mol^{-1})	ΔS/ (J mol^{-1} K^{-1})	ΔG/(kJ mol^{-1})		
			293 K	303 K	313 K
8.01	44.7	0.170	−5.86	−7.23	−9.30

It can be seen from the data in the table that $\Delta G < 0$, $\Delta H > 0$, $\Delta S > 0$, indicating that the adsorption process is an endothermic and entropy-increasing spontaneous reaction [36]. $\Delta H < 84$ kJ mol^{-1} and $E_a < 40$ kJ mol^{-1} proves that the adsorption process of Zr-DWS to AR is a process of spontaneous endothermic entropy increase and contains physical adsorption.

3.2.7. Competitive adsorption of AK and AR

The adsorption amount of both was calculated, and then the adsorption constant was calculated. The results are shown in Table 5.

It can be seen from Table 5 that the adsorption capacity of Zr-DWS for AR and AK is 173 and 90.0 mg g^{-1}, respectively; however the adsorption capacity of AR and AK by Zr-DWS both decreased during mixed adsorption. The adsorption capacity of AR was only reduced by 27.6%, while the adsorption capacity of AK was reduced by 38.3%. This shows that the adsorption mechanism of Zr-DWS to the two adsorbates is different, and the adsorption of AR to Zr-DWS is mainly complexation. The dissociation constant for AR is much larger than AK, which fully shows that Zr-DWS has preferential selectivity for AR.

3.3. Column adsorption research

3.3.1. Effect of column height

The effects of bed height on breakthrough curves are presented in Fig. 9. It can be seen from the graph that the higher the column is, the smaller the slope of the outflow curve of AR adsorption by Zr-DWS, and the longer the time to reach adsorption saturation. This is because with the increase of the column, there are more adsorbents Zr-DWS in the column, and more active sites can adsorb AR, which makes the adsorption reach equilibrium for a longer time.

3.3.2. Effect of flow rate

The breakthrough curves at various flow rates are shown in Fig. 9. It was clearly noticed that when the column height and solution concentration are constant, the greater the flow rate, the greater the slope of AR adsorption outflow curve of Zr-DWS, and the shorter the adsorption saturation time. At the same time, the total adsorption quantity becomes smaller and the removal rate becomes worse. This is because the contact time between AR and adsorbent Zr-DWS in the column is shorter with the increase of flow rate, which makes the opportunity of binding between adsorbate AR and active sites smaller, so the adsorption quantity becomes smaller.

3.3.3. Effect of concentration

The shapes of breakthrough curves are also related to adsorbate concentration and the results are shown in Fig. 9. It can be seen that the greater the concentration, the greater the slope of the outflow curve, and the shorter the time to reach adsorption saturation.

The corresponding quantities were calculated according to Eqs. (3)–(6), and the results are shown in Table 6. From the data set 2, 4, and 5 in Table 6, it is shown that when the column height and flow rate are constant, the higher the solution concentration, the larger the total adsorption capacity of Zr-DWS for AR adsorption, but the removal rate decreases. This is consistent with the effect of flow rate on the adsorption of Zr-DWS on AR. Therefore, high concentration is not as good as low concentration. It was also observed that the removal efficiency is not higher for whole

Table 5
Comparison of Adsorption of AK and AR by Zr-DWS

Adsorbent	Single system	Binary system	Decrement	Adsorption constant
	q_e (mg g^{-1})	q_e (mg g^{-1})	%	K_d
AR	173	126	27.6	1.39
AK	90.0	55.5	38.3	0.54

Note: $K_d = q_e/C_e$.

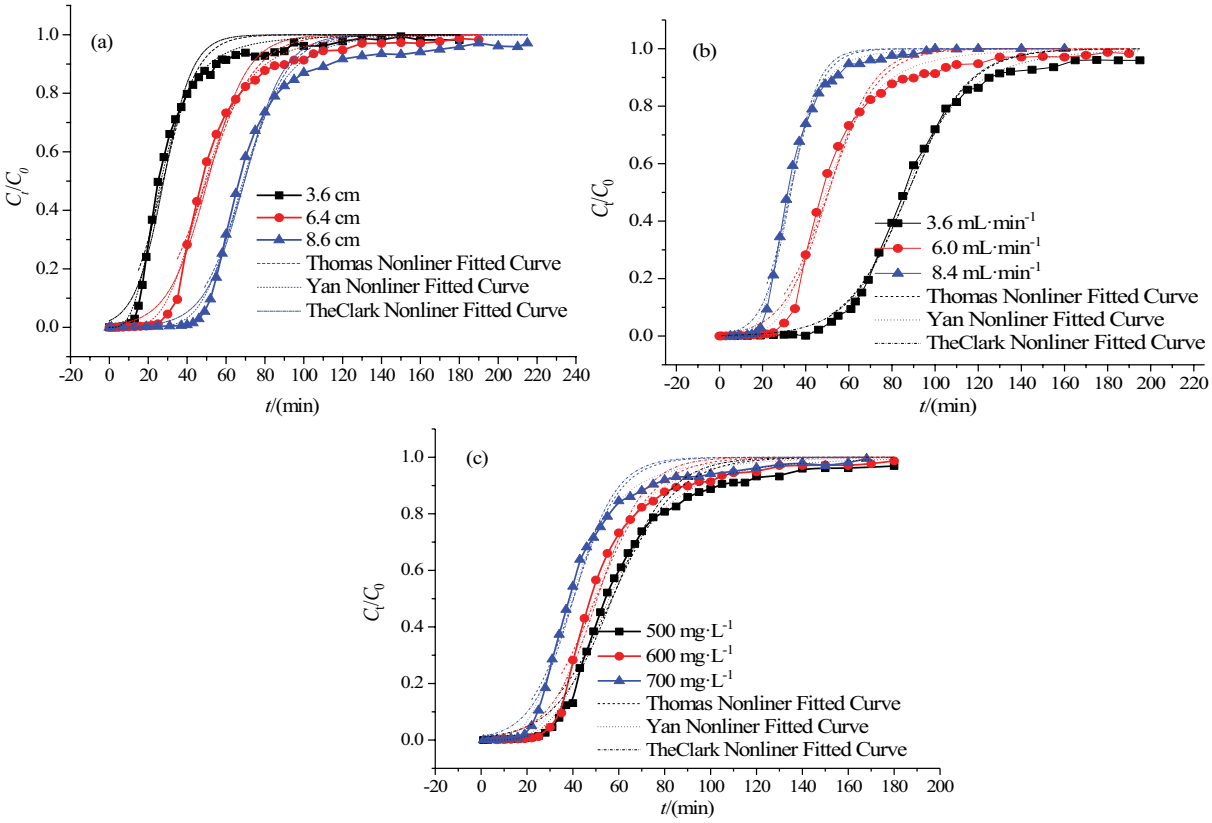

Fig. 9. Breakthrough curves of AR adsorption onto Zr-DWS at various conditions (a, b, c are column height, flow rate, concentration, respectively).

breakthrough curves and there was no significant difference in adsorption quantity (mg g^{-1}).

It was also found the values of q_e in Table 6 were over the results from batch experiments listed in Tables 2 and 3. The reason was due to the difference of solution pH. The column mode is at pH = 3, which is in favor of AR adsorption.

3.3.4. Model fitting of column adsorption curve

In order to discuss the equilibrium adsorption capacity and adsorption characteristic parameters of Zr-DWS for AR adsorption under different conditions, this experiment continued to fit the adsorption process with these models, and the fitting results are shown in Table 7 and Fig. 9.

Thomas model can predict the maximum theoretical adsorption capacity of AR by Zr-DWS, but its disadvantage is that it cannot fit the initial stage of column adsorption process, and Yan model can make up for this defect. However, the Yan model cannot directly fit the unit adsorption capacity q_e (mg g^{-1}), but it can be obtained according to the model parameter b by the following formula:

Table 6
Column adsorption data of AR by Zr-DWS

Z/(cm)	v/(mL min^{-1})	C_0/(mg L^{-1})	Q_m/(mg)	W_{total}/(mg)	Y/(%)	q_e/(mg g^{-1})
3.6	6.0	600	115	360	19.8	265
6.4	6.0	600	198	468	45.1	273
8.6	6.0	600	274	648	60.7	270
6.4	6.0	500	195	420	46.4	269
6.4	6.0	700	189	504	37.5	260
6.4	3.6	600	198	389	53.2	273
6.4	8.4	600	175	353	49.7	242

Table 7
Model nonlinear fitting results of Zr-DWS on AR column adsorption

Thomas							
Z/cm	v/(mL min^{-1})	C_0/(mg L^{-1})	K_{Th}/(mL mg^{-1} min^{-1})	$q_{e(exp)}$/(mg g^{-1})	$q_{e(theo)}$/(mg g^{-1})	R^2	SSE × 10^2
3.6	6	600	0.187 ± 0.015	265	99.2 ± 2.5	0.957	8.60
6.4	6	600	0.132 ± 0.012	273	182 ± 4	0.952	5.90
8.6	6	600	0.150 ± 0.013	270	250 ± 4	0.966	7.40
6.4	6	500	0.142 ± 0.010	269	171 ± 3	0.965	7.60
6.4	6	700	0.142 ± 0.011	260	169 ± 3	0.970	6.60
6.4	4	600	0.118 ± 0.005	273	189 ± 2	0.989	2.90
6.4	8	600	0.142 ± 0.010	242	166 ± 2	0.984	3.00
Yan							
Z/cm	v/(mL min^{-1})	C_0/(mg L^{-1})	A	b/mL	$q_{e(theo)}$/(mg g^{-1})	R^2	SSE × 10^2
3.6	6	600	3.31 ± 0.11	159 ± 2	219	0.995	2.90
6.4	6	600	4.46 ± 0.19	296 ± 3	244	0.995	2.90
8.6	6	600	6.28 ± 0.32	412 ± 4	244	0.992	4.80
6.4	6	500	4.16 ± 0.13	335 ± 3	231	1.00	2.50
6.4	6	700	3.95 ± 0.12	235 ± 2	226	0.996	2.00
6.4	4	600	6.01 ± 0.12	309 ± 1	256	0.998	0.900
6.4	8	600	4.92 ± 0.13	271 ± 2	225	0.998	1.00
The Clark							
Z/cm	v/(mL min^{-1})	C_0/(mg L^{-1})	n	r × 10^{-2}	A	R^2	SSE × 10^2
3.6	6	600	2	1.35 ± 1.00	43.0 ± 12	0.977	12.3
6.4	6	600	2	9.75 ± 0.73	138 ± 52	0.986	8.60
8.6	6	600	2	9.80 ± 0.72	910 ± 44	0.985	8.70
6.4	6	500	2	8.03 ± 0.50	98.6 ± 28	0.982	10.0
6.4	6	700	2	10.9 ± 0.7	80.9 ± 24	0.985	8.20
6.4	4	600	2	7.25 ± 0.30	584 ± 15	0.994	3.20
6.4	8	600	2	15.8 ± 0.9	187 ± 57	0.991	4.60

$$q_e = \frac{bC_0}{m} \quad (15)$$

where b (mL) is the Yan model parameter, C_0 (mg L^{-1}) is the initial concentration of AR, and m (g) is the mass of Zr-DWS.

The Clark model is a column adsorption model combined with batch state, where n is the fitted parameter in the Freundlich model in the batch model.

It can be seen from Table 7 that $q_{e(theo)}$ and $q_{e(exp)}$ change with the change of column height, flow rate and initial concentration of AR, and the R^2 values fitted by Thomas, Yan and The Clark models are all greater than 0.960, but the R^2 values fitted by Yan model are larger, SSE is smaller, and the difference between theoretical adsorption capacity and actual adsorption capacity is small. Therefore, Yan model is more suitable for describing the adsorption behavior.

3.4. Desorption and regeneration experiment

3.4.1. Batch desorption and regeneration

Desorption research helps explain the adsorption mechanism and makes the adsorption process more economical [37,38]. The adsorbent was cleaned and dried, and desorption experiments were carried out with 0.1 mol L^{-1} NaOH, 0.01 mol L^{-1} NaOH, 0.1 mol L^{-1} HCl, 25% ethanol, 0.01 mol L^{-1} NaCl and water, respectively, and the desorption rate d was calculated. Then, the adsorbent is cleaned to neutral surface and dried for re-adsorption experiment, and the regeneration rate r is calculated, and the result is shown in Fig. 10. The desorption method with the best desorption effect was selected, and three desorption regeneration experiments were carried out, and the results are shown in Fig. 11. When the pH of the solution is not adjusted, the interaction between adsorbent and adsorbate mainly depends on complexation and electrostatic attraction. Therefore, the existence of −OH will destroy the force between them and make the desorption rate higher. It can be seen from Fig. 10 that 0.1 mol L^{-1} NaOH has good desorption regeneration effect three times, with desorption rates of 73.7%, 50.5% and 48.9%, respectively. The regeneration rates are 60.1%, 59.9% and 58.3%, respectively, which indicates that Zr-DWS can be recycled for many times (Fig. 11).

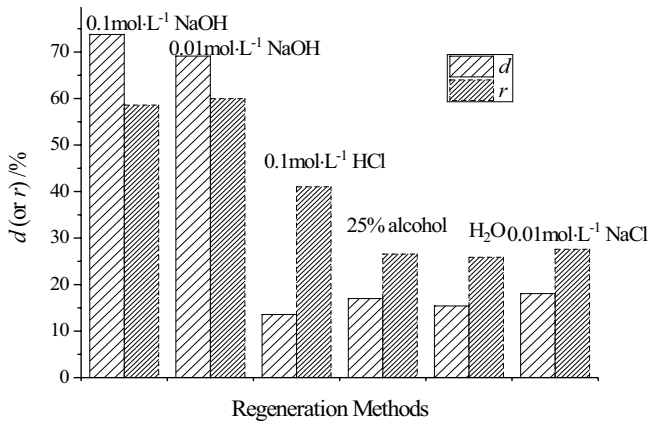

Fig. 10. Comparison of several desorption methods.

3.4.2. Column desorption and regeneration

Under the conditions of column height Z = 6.4 cm, pH = 3, C_0 = 600 mg L^{-1} AR solution, flow rate v = 6.0 mL min^{-1}, the column adsorption experiment was carried out to make Zr-DWS reach adsorption saturation, and the adsorbent saturated with adsorbate was regenerated (the flow rate was controlled, the column height was the same as the adsorption experiment), and the AR in effluent was measured. Select the best desorption solution in batch adsorption and desorption with the concentration C_t of 0.1 mol L^{-1}, until the concentration of AR in the effluent is basically unchanged. The above adsorption and desorption experiments are repeated, and the column desorption curve is plotted by C_t vs. time t, as shown in Fig. 12. The column regeneration adsorption curve is plotted with C_t/C_0 vs. time t, as shown in Fig. 13.

According to the integration of Figs. 12 and 13, it is calculated that the initial adsorption capacity of Zr-DWS for AR was 273 mg g^{-1}, values of d about twice desorption were 28.5% and 35.0% while the regeneration adsorption capacity was 203 and 195 mg g^{-1}, respectively. The values of r were 74.5% and 71.4%, respectively. It can be seen that Zr-DWS is not easy to desorb AR after AR adsorption, which is consistent with the conclusion of batch experiment.

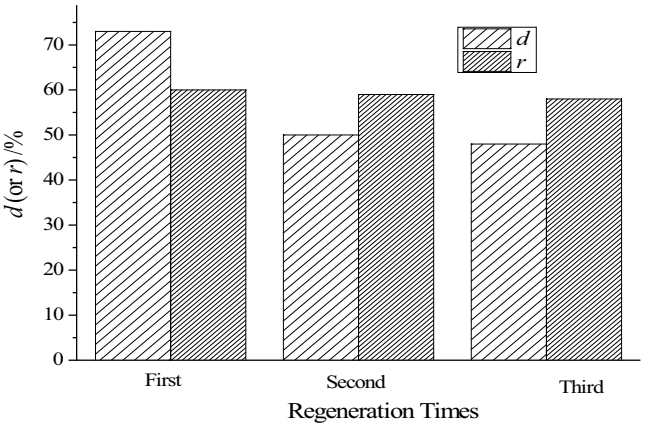

Fig. 11. Results of three regenerations using 0.1 mol L^{-1} NaOH.

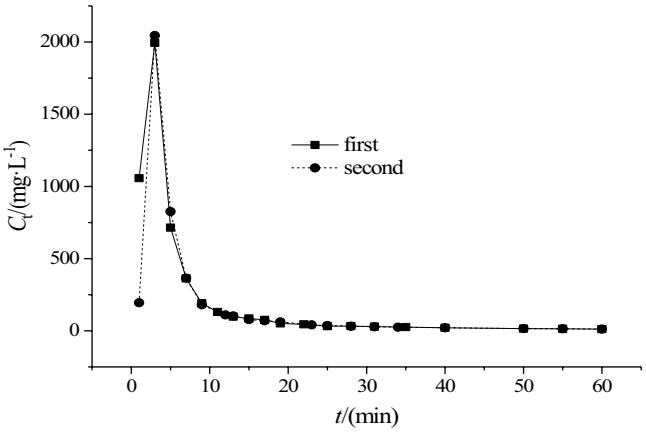

Fig. 12. Column desorption curve of Zr-DWS.

3.5. Comparison with other materials

In order to show that the adsorbent prepared in this study has a good effect, this study extracts the adsorption of other adsorbents to water pollutants, which are listed in Table 8. Several factors can affect the adsorption quantity, such as solution pH, temperature, etc. The adsorption quantity of Zr-DWS toward AR was 164 mg g^{-1} from batch study. So there is some competitive advantage about application of Zr-DWS because there is higher adsorption capacity and selection toward AR from mixtures.

3.6. Adsorption mechanism

In this experiment, XPS analysis was performed on Zr-DWS adsorption of AR, and the results are shown in Figs. 14 and 15. Fig. 14 is the XPS full spectrum before and after adsorption, and Fig. 15 is the XPS of O1s and Zr3d after AR adsorption.

Comparing the full spectrum before and after AR adsorption in Fig. 14, it can be seen that after AR adsorption, there is an obvious S2p peak at 168 eV. This is the energy spectrum peak of S in AR adsorbed to the surface of Zr-DWS, indicating that AR is successful adsorbed to Zr-DWS.

There are three main peaks in the O1s peak diagram of Zr-DWS before and after AR adsorption in Fig. 15. The energies from small to large correspond to the bonding of O^{2-}, Zr–O/–OH, and H_2O. Comparing the O1s peak diagrams before and after adsorption, it can be seen that the proportion of OH/Zr–O increased from 80.2% to 84.2%, and the proportion of H_2O decreased from 13.05% to 5.4%, which indicates that the water complexed on Zr on the surface of Zr-DWS combined with the –OH of AR. According to the structure of AR, it can be seen that the Zr supported on the surface of Zr-DWS may form a four-coordinate compound with the adjacent hydroxyl group of AR. Comparing the Zr3d peak maps before and after adsorption, it is found that there are more Zr–O bonds after adsorption, which is consistent with the results obtained by O1s.

Combined with the study of the process of AR adsorption by Zr-DWS, it can be speculated that the adsorption mechanism of Zr-DWS on AR is mainly electrostatic attraction and complexation; in addition, this paper uses xylenol orange spectrophotometry to calculate the zirconium loading of DWS in this experiment as 37.1 mg g^{-1}, then the mass ratio of zirconium to AR is calculated as 0.8, which is approximately a 1:1 reaction, so a zirconium reacts with two adjacent hydroxyl groups on an AR. Under the pH conditions of the reaction, the surface of Zr-DWS is positively charged, and there is electrostatic attraction between the negatively charged anionic dye AR. The complexation process between Zr-DWS and AR is shown in Fig. 16, forming a four-coordination compound.

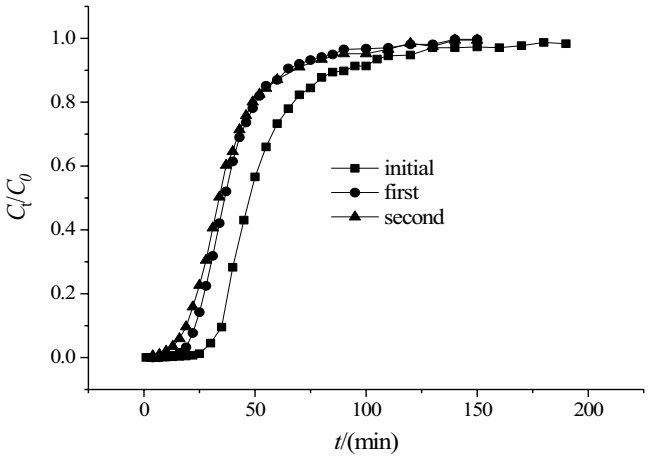

Fig. 13. Column regenerative adsorption curve of Zr-DWS.

4. Conclusion

In this study, an efficient and environmental friendly adsorbent, Zr-DWS, was prepared and the adsorption property toward AR was performed in batch mode and column mode. The modification method visibly improved the ability of wheat straw. The coexisting salt ions basically had no effect on the adsorption while the temperature had a positive effect on the adsorption. The Koble–Corrigan model was most suitable to describe the adsorption process while the adsorption process conformed to pseudo-second-order kinetic model. There is favor of AR adsorption with the higher adsorbate concentration, and the slower flow rate. Yan model could well describe the column adsorption behavior. In addition, Zr-DWS had obvious selectivity for AR removal. To sum up, Zr-DWS, which has excellent properties such as strong adsorption capacity, convenient separation, and reusability, is promising to remove some anionic pollutants from mixtures.

Table 8
Comparison of the quantity adsorbed by different adsorbents for the removal of AR

Adsorbents	Adsorption capacity q_e/(mg g^{-1})	Ref
Modified magnetic peanut husk	49.4	[33]
Zr(IV)-loaded graphene oxide	231	[39]
Zr(IV) hydroxide coated magnetic materials	83.7	[40]
Magnetic chitosan	40.1	[41]
PEI modified magnetic carbon nanotubes	196	[42]
$NiFe_2O_4$/polyaniline (PANI) magnetic composite	186	[43]
Activated biocarbon from pine core	118	[44]
Zr-DWS	164	This work

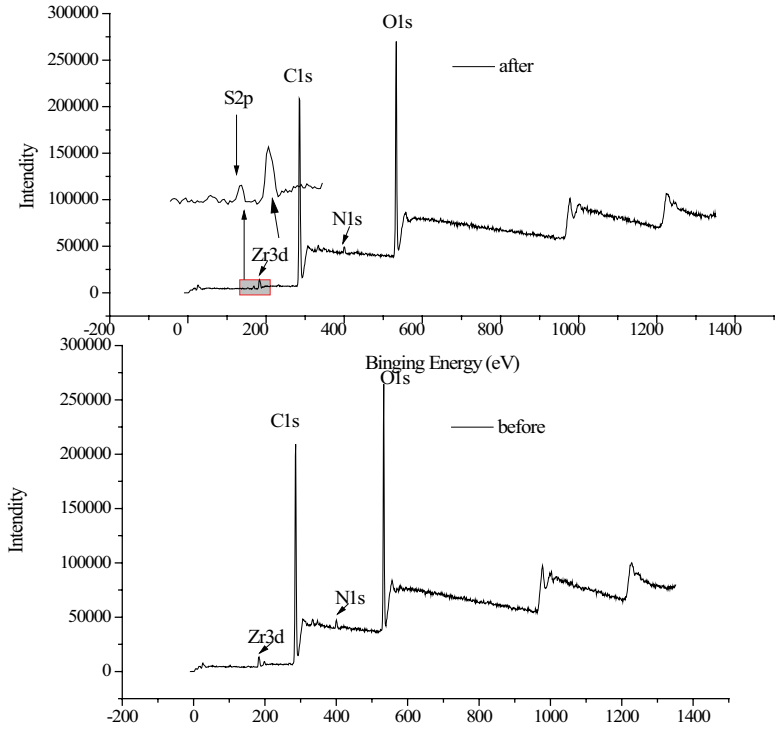

Fig. 14. Comparison of XPS full spectrum before and after Zr-DWS adsorption of AR.

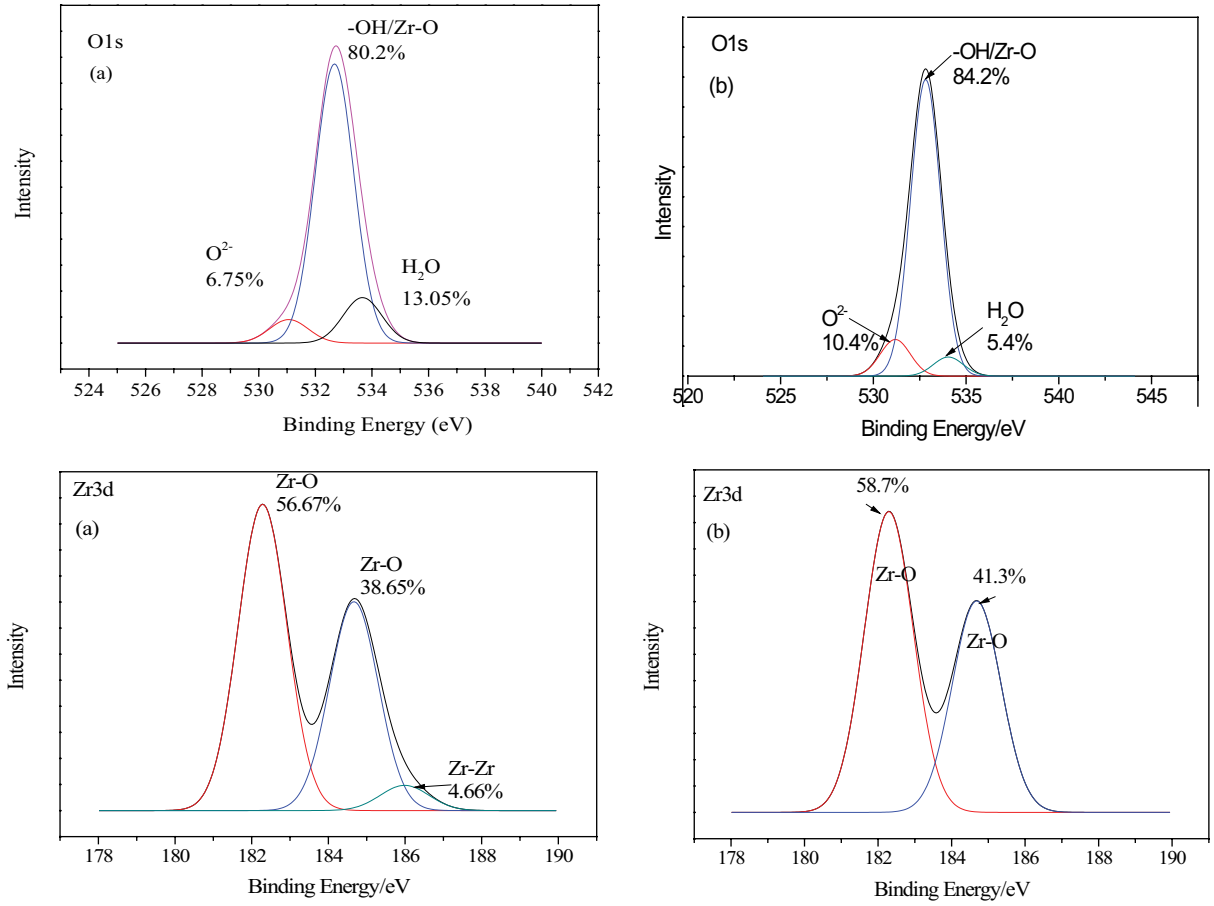

Fig. 15. XPS of O1s and Zr3d before and after AR adsorption by Zr-DWS (a is before adsorption, b is after adsorption).

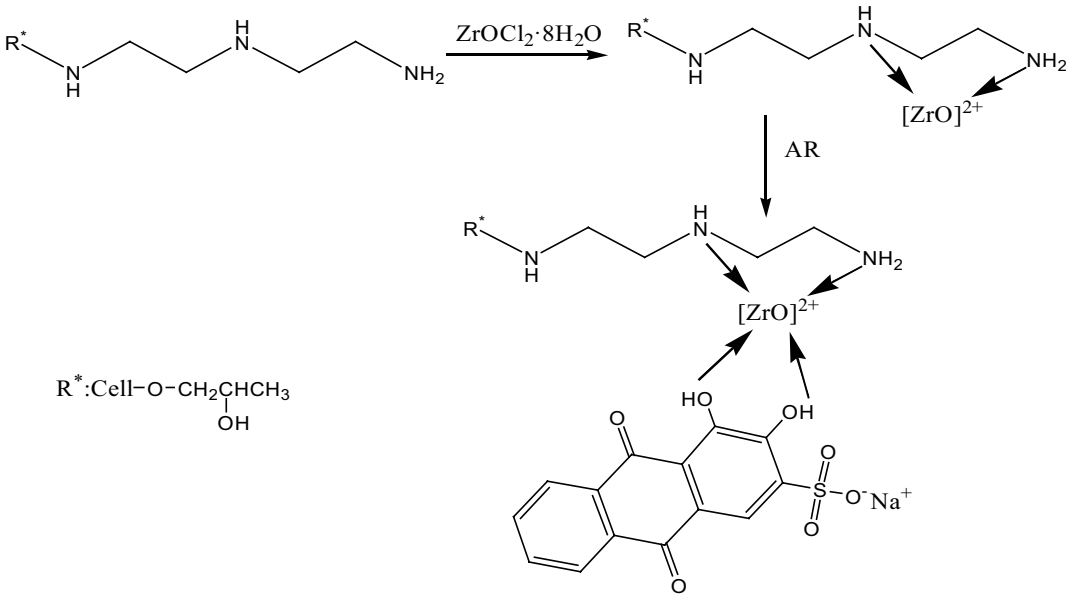

Fig. 16. Complex mechanism diagram of Zr-DWS adsorption of AR.

Acknowledgments

This work was financially supported by the Henan province basis and advancing technology research project (142300410224).

References

[1] G. Crini, E. Lichtfouse, L.D. Wilson, N. Morin-Crini, Conventional and non-conventional adsorbents for wastewater treatment, Environ. Chem. Lett., 17 (2019) 1951213.
[2] F.M. Mpatani, A.A. Aryee, A.N. Kani, R.P. Han, Z.H. Li, E. Dovi, L.B. Qu, A review of treatment techniques applied for selective removal of emerging pollutant-trimethoprim from aqueous systems, J. Clean. Prod., 308 (2021) 127359.
[3] I. Hamawand, A. Ghadouani, J. Bundschuh, S. Hamawand, R.A. Al Juboori, S. Chakrabarty, T. Yusaf, A critical review on processes and energy profile of the Australian meat processing industry, Energies, 10 (2017) 731.
[4] P. Anastasio, T. Del Giacco, R. Germani, N. Spreti, M. Tiecco, Structure effects of amphiphilic and non-amphiphilic quaternary ammonium salts on photodegradation of Alizarin Red-S catalyzed by titanium dioxide, RSC Adv., 7 (2017) 361–368.
[5] F.M. Machado, S.A. Carmalin, E.C. Lima, S.L.P. Dias, L.D.T. Prola, C. Saucier, I.M. Jauris, I. Zanella, S.B. Fagan, Adsorption of alizarin red S dye by carbon nanotubes: an experimental and theoretical investigation, J. Phys. Chem. C, 120 (2016) 18296–18306.
[6] M.B. Gholivand, Y. Yamini, M. Dayeni, S. Seidi, E. Tahmasebi, Adsorptive removal of alizarin red-S and alizarin yellow GG from aqueous solutions using polypyrrole-coated magnetic nanoparticles, J. Environ. Chem. Eng., 3 (2015) 529–540.
[7] C.A. Martínez-Huitle, E. Brillas, Decontamination of wastewaters containing synthetic organic dyes by electrochemical methods: a general review, Appl. Catal. B, 87 (2009) 105–145.
[8] F. Zhang, B. Ma, X. Jiang, Y. Ji, Dual function magnetic hydroxyapatite nanopowder for removal of malachite green and Congo red from aqueous solution, Powder Technol., 302 (2016) 207–214.
[9] Z. Askarniya, M.T. Sadeghi, S. Baradaran, Decolorization of Congo red via hydrodynamic cavitation in combination with Fenton's reagent, Chem. Eng. Process, 150 (2020) 107874.
[10] F. Mashkoor, A. Nasar, Inamuddin, A.M. Asiri, Exploring the reusability of synthetically contaminated wastewater containing crystal violet dye using tectona grandis sawdust as a very low-cost adsorbent, Sci. Rep., 8 (2018) 8314.
[11] J. Mo, Q. Yang, N. Zhang, W. Zhang, Y. Zheng, Z. Zhang, A review on agro-industrial waste (AIW) derived adsorbents for water and wastewater treatment, J. Environ. Manage., 227 (2018) 395–405.
[12] X. Liu, D.J. Lee, Thermodynamic parameters for adsorption equilibrium of heavy metals and dyes from wastewaters, Bioresour. Technol., 160 (2014) 24–31.
[13] M. Min, L. Shen, G. Hong, M. Zhu, Y. Zhang, X. Wang, Y. Chen, B.S. Hsiao, Micro-nano structure poly(ether sulfones)/poly(ethyleneimine) nanofibrous affinity membranes for adsorption of anionic dyes and heavy metal ions in aqueous solution, Biochem. Eng. J., 197 (2012) 88–100.
[14] K. Dong, T. Hu, G. Wei, Q. Liu, T. Gao, X. Zhang, J. Yao, Removal of hexavalent chromium from aqueous solution using novel dye-based adsorbent prepared by flocculation, Sep. Sci. Technol., 54 (2019) 1739–1748.
[15] Y.J. Shih, C.P. Lin, Y.H. Huang, Application of Fered-Fenton and chemical precipitation process for the treatment of electroless nickel plating wastewater, Sep. Purif. Technol., 104 (2013) 100–105.
[16] T. Sun, Z. Zhao, Z. Liang, J. Liu, W. Shi, F. Cui, Efficient removal of arsenite through photocatalytic oxidation and adsorption by ZrO_2-Fe_3O_4 magnetic nanoparticles, Appl. Surf. Sci., 416 (2017) 656–665.
[17] F.M. Mpatani, R.P. Han, A.A. Aryee, A.N. Kani, Z.H. Li, L.B. Qu, Adsorption performance of modified agricultural waste materials for removal of emerging micro-contaminant bisphenol A: a comprehensive review, Sci. Total Environ., 780 (2021) 146629.
[18] A.A. Aryee, F.M. Mpatani, Al.N. Kani, E. Dovi, R.P. Han, Z.H. Li, L.B. Qu, A review on functionalized adsorbents based on peanut husk for the sequestration of pollutants in wastewater: modification methods and adsorption study, J. Clean. Prod., 310 (2021) 127502.
[19] I. Ali, C. Peng, I. Naz, D. Lin, D.P. Saroj, M. Ali, Development and application of novel bio-magnetic membrane capsules for the removal of the cationic dye malachite green in wastewater treatment, RSC Adv., 9 (2019) 3625–3646.
[20] R. Lafi, I. Montasser, A. Hafiane, Adsorption of congo red dye from aqueous solutions by prepared activated carbon with

oxygen-containing functional groups and its regeneration, Adsorpt. Sci. Technol., 37 (2018) 160–181.
[21] W. Li, X. Liao, L. Wang, Z. Huang, Adsorption of cadmium and lead in wastewater by four kinds of biomass xanthates, Water Sci. Technol., 79 (2019) 1222–1230.
[22] A.A. Amin, Phosphorus dynamics and corn growth under applications of corn stalks biochar in a clay soil, Arab. J. Geosci., 11 (2018) 379.
[23] N. Kaya, A comprehensive study on adsorption behavior of some azo dyes from aqueous solution onto different adsorbents, Water Sci. Technol., 76 (2017) 478–489.
[24] P. Kaur, P. Kaur, K. Kaur, Adsorptive removal of imazethapyr and imazamox from aqueous solution using modified rice husk, J. Clean. Prod., 244 (2020) 118699.
[25] J. Zhang, Q. Zhou, L. Ou, Removal of indigo carmine from aqueous solution by microwave-treated activated carbon from peanut shell, Desal. Wat. Treat., 57 (2016) 718–727.
[26] Y.J. Wu, L.J. Zhang, C.L. Gao, J.Y. Ma, X.H. Ma, R.P. Han, Adsorption of copper ions and methylene blue in a single and binary system on wheat straw, J. Chem. Eng. Data, 54 (2009) 3229–3234.
[27] M. Wu, H. Liu, C. Yang, Effects of pretreatment methods of wheat straw on adsorption of Cd(II) from waterlogged paddy soil, Int. J. Environ. Res. Public Health, 16 (2019) 205.
[28] Y.Y. Su, B.L. Zhao, W. Xiao, R.P. Han, Adsorption behavior of light green anionic dye using cationic surfactant-modified wheat straw in batch and column mode, Environ. Sci. Pollut. Res., 20 (2013) 5558–5568.
[29] R.P. Han, L.J. Zhang, C. Song, M.M. Zhang, H.M. Zhu, L.J. Zhang, Characterization of modified wheat straw, kinetic and equilibrium study about copper ion and methylene blue adsorption in batch mode, Carbohydr. Polym., 79 (2010) 1140–1149.
[30] Y. Zhan, H. Zhang, J. Lin, Z. Zhang, J. Gao, Role of zeolite's exchangeable cations in phosphate adsorption onto zirconium-modified zeolite, J. Mol. Liq., 243 (2017) 624–637.
[31] Y. Su, H. Cui, Q. Li, S. Gao, J.K. Shang, Strong adsorption of phosphate by amorphous zirconium oxide nanoparticles, Water Res., 47 (2013) 5018–5026.
[32] N.Y. Acelas, B.D. Martin, D. López, B. Jefferson, Selective removal of phosphate from wastewater using hydrated metal oxides dispersed within anionic exchange media, Chemosphere, 119 (2015) 1353–1360.
[33] A.A. Aryee, E. Dovi, Q. Guo, M. Liu, R.P. Han, Z.H. Li, L. Qu, Selective removal of anionic dyes in single and binary system using Zirconium and iminodiacetic acid modified magnetic peanut husk, Environ. Sci. Pollut. Res., 28 (2021) 37322–37337.
[34] M.J. Ahmed, B.H. Hameed, E.H. Hummadi, Insight into the chemically modified crop straw adsorbents for the enhanced removal of water contaminants: a review, J. Mol. Liq., 330 (2021) 115616.
[35] Y. Chun, G. Sheng, C.T. Chiou, B. Xing, Compositions and sorptive properties of crop residue-derived chars, Environ. Sci. Technol., 38 (2004) 4649–4655.
[36] H.N. Bhatti, A. Jabeen, M. Iqbal, S. Noreen, Z. Naseem, Adsorptive behavior of rice bran-based composites for malachite green dye: Isotherm, kinetic and thermodynamic studies, J. Mol. Liq., 237 (2017) 322–333.
[37] B.L. Zhao, W. Xiao, Y. Shang, H.M. Zhu, R.P. Han, Adsorption of light green anionic dye using cationic surfactant-modified peanut husk in batch mode, Arab. J. Chem., 10 (2017) S3595–S3602.
[38] A.A. Aryee, E. Dovi, R.P. Han, Z.H. Li, L.B. Qu, One novel composite based on functionalized magnetic peanut husk as adsorbent for efficient sequestration of phosphate and Congo red from solution: characterization, equilibrium, kinetic and mechanism studies, J. Colloid Interface Sci., 598 (2021) 69–82.
[39] M.Y. Liu, X.T. Zhang, Z.H. Li, L.B. Qu, R.P. Han, Fabrication of zirconium (IV)-loaded chitosan/Fe_3O_4/graphene oxide for efficient removal of alizarin red from aqueous solution, Carbohydr. Polym., 248 (2020) 116792.
[40] Y.Y. Hu, R.P. Han, Selective and efficient removal of anionic dyes from solution by Zirconium(IV) hydroxide-coated magnetic materials, J. Chem. Eng. Data, 64 (2019) 791–799.
[41] L.L. Fan, Y. Zhang, X.J. Li, C.N. Luo, F.G. Lu, H.M. Qiu, Removal of alizarin red from water environment using magnetic chitosan with Alizarin Red as imprinted molecules, Colloid Surf. B, 91 (2012) 250–257.
[42] Z.F. Zhang, H.J. Chen, W.M. Wu, W.T. Pang, G.Q. Yan, Efficient removal of Alizarin Red S from aqueous solution by polyethyleneimine functionalized magnetic carbon nanotubes, Bioresour. Technol., 293 (2019) 122100.
[43] Y.D. Liang, Y.J. He, Y.H. Zhang, Q.Q. Zhu, Adsorption property of alizarin red S by $NiFe_2O_4$/polyaniline magnetic composite, J. Environ. Chem. Eng., 6 (2018) 416–425.
[44] P.C. Bhomick, A. Supong, M. Baruah, C. Pongener, D. Sinha, Pine Cone biomass as an efficient precursor for the synthesis of activated biocarbon for adsorption of anionic dye from aqueous solution: Isotherm, kinetic, thermodynamic and regeneration studies, Sust. Chem. Pharm., 10 (2018) 41–49.